The Effect of Midlatitude Transient Eddies on Monsoonal Southerlies over Eastern China

HYO-SEOK PARK

Korea Institute of Geoscience and Mineral Resources, Daejeon, South Korea

BENJAMIN R. LINTNER

Department of Environmental Sciences, Rutgers, The State University of New Jersey, New Brunswick, New Jersey

WILLIAM R. BOOS

Department of Geology and Geophysics, Yale University, New Haven, Connecticut

KYONG-HWAN SEO

Department of Atmospheric Sciences, Pusan National University, Busan, South Korea

(Manuscript received 13 February 2015, in final form 19 June 2015)

ABSTRACT

The strengthening of monsoonal southerlies over East Asia is associated with the westward intensification of the North Pacific subtropical high. Previous work has shown that the seasonal-mean position and strength of subtropical highs are affected by tropical and subtropical diabatic heating. Here it is shown that the synoptic-time-scale strengthening of southerlies over eastern China is dynamically tied to extratropical eddy activity. Composite analysis based on strong southerly wind events highlights an antecedent baroclinic wave train propagating southeastward into eastern China from extratropical central Asia. This wave train generates quasigeostrophic ascent over eastern China that is associated with heavy precipitation. The anomalously cold upper-tropospheric conditions associated with the wave train decrease static stability throughout the lower and middle troposphere in eastern China, while low-level moistening enhances equivalent potential temperature. It is proposed that the resulting reductions in dry and moist static stability intensify the eddy-induced precipitating ascent. These results illustrate how East Asian monsoon circulation and precipitation can be enhanced by the interaction of midlatitude baroclinic waves with the moist subtropical monsoon region.

1. Introduction

The annual cycle of rainfall over East Asia is characterized by relatively dry winters and rainy springs and summers, with the summer season (June–August) rainfall often referred to as the East Asian summer monsoon (EASM). In early summer (June–July), strong low-level southerlies develop over East Asia and a zonally elongated precipitation band appears over south-central China, South Korea, and southern Japan (Fig. 1c). This rainband, known as the mei-yu–baiu (MB) front, generally forms on the northern boundary of a warm subtropical air mass (Kodama 1992). To the north of the MB, a strong upper-tropospheric westerly jet develops (contours in Fig. 1a) and plays a key role in the seasonal evolution of the EASM (e.g., Zhang et al. 2006). This MB is quasi-stationary (e.g., Ninomiya 1984) and has its maximum impact over East Asia in June and July (Liang and Wang 1998; Ding and Chan 2005; Zhou et al. 2009b; Seo et al. 2012). In late July, the westerly jet weakens and its core shifts northeastward (Schiemann et al. 2009; Zhang et al. 2006), while the MB transitions to more sporadic and transient precipitation events (e.g., Molnar et al. 2010; Sampe and Xie 2010). The position and intensity of the MB exhibits large variability on various time scales, which can exert strong impacts on natural and human systems in the densely populated East Asian

Corresponding author address: Hyo-Seok Park, Korea Institute of Geoscience and Mineral Resources, 124 Gwahak-ro, Yuseong-gu, Daejeon 305-350, South Korea.
E-mail: hspark1@gmail.com

DOI: 10.1175/JCLI-D-15-0133.1

© 2015 American Meteorological Society

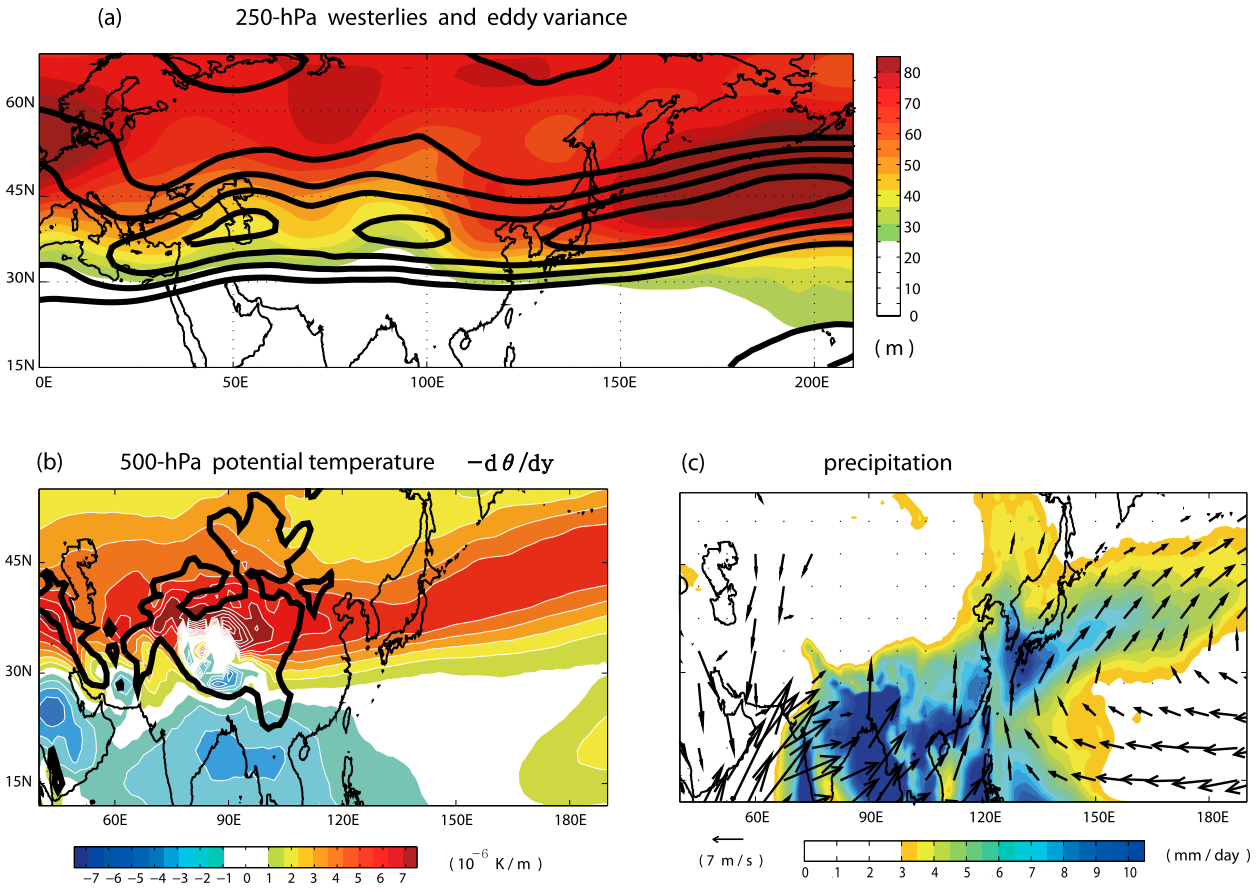

FIG. 1. June–July mean (a) eddy geopotential height variance $(Z'^2)^{1/2}$ (shading; m) and westerly wind speed (contours from 10 m s^{-1} with interval of 5 m s^{-1}) at 250 hPa. (b) Meridional gradients of potential temperature (10^{-6} K m^{-1}) at 500 hPa and (c) precipitation (shadings; mm day^{-1}) and 925-hPa winds (m s^{-1}). Wind vectors >2.0 m s^{-1} are plotted. Thick contours in (b) indicate topography >1200 m. All data are from ERA-Interim, except the precipitation in (c), which is from GPCP.

region. For example, the development of strong monsoonal southerlies over eastern China is often followed by the northward shift of the rainband, producing excessive precipitation over northern China (Zhou et al. 2009b), a region that is otherwise vulnerable to drought (Wang 2006).

The presence of a quasi-steady subtropical high pressure system over the western North Pacific, the North Pacific subtropical high (NPSH), is regarded as key to maintaining the monsoonal southerlies (Kodama 1992; Zhou et al. 2009a; Wu et al. 2010; Wang et al. 2013). The time-mean position and intensity of the NPSH are connected to sea surface temperatures (SSTs) and the associated diabatic heating field (Liu et al. 2004; Zhou et al. 2009b; Wu et al. 2010; Song and Zhou 2014a). Westward intensification of the NPSH associated with spatial redistribution of SSTs and the diabatic heating field is thought to control the interannual variability of monsoonal southerlies and precipitation over eastern China (Zhou et al. 2009a; Wu et al. 2010; Wang et al. 2013). Specifically, anomalously warm SSTs over the tropical Indian Ocean and cold SSTs in the tropical central Pacific can induce the westward intensification of the NPSH (Wang et al. 2000; Yang et al. 2007; Li et al. 2008; Wang et al. 2013; Song and Zhou 2014b).

While diabatic heating is a fundamental driver for subtropical circulations in the summer, the presence of westerlies is essential for the generation of Rossby waves and the associated subtropical highs such as the NPSH (Rodwell and Hoskins 2001). The position and strength of westerlies are sensitive to tropical diabatic heating (Yang and Webster 1990; Ting 1994), indicating that the mean-state properties that affect wave propagation respond to changes in the diabatic heating field. It is thus natural to ask whether extratropical eddies, superimposed on westerlies, can affect subtropical circulations. Indeed, previous studies consistently suggest that subtropical circulations are influenced by extratropical eddies occurring in baroclinic zones, even in the summer (e.g., Enomoto et al. 2003; Kosaka et al. 2009;

Kang and Lu 2012). For example, Song and Zhou (2013) showed that synoptic-scale transient eddy activity contributed to bias in the simulation of the time-mean East Asian subtropical jet.

The extratropical baroclinic nature of the EASM is evident in the frontal nature of the MP precipitation maximum. Figure 1a depicts 250-hPa westerlies (contours) and the synoptic-scale eddy activity (shading), defined as the variance of 250-hPa eddy geopotential height $(Z'^2)^{1/2}$, where the prime denotes 10-day high-pass-filtered values). The subtropical jet speed has a local maximum over the Tibetan Plateau, between 50° and 100°E and 35° and 45°N, whereas the transient eddy activity peaks at higher latitudes, between 45° and 60°N. While the transient eddy activity is relatively weak over the Tibetan Plateau, the (mean) meridional potential temperature gradient $-\partial_y\overline{\theta}$ at 500 hPa is largest there (Fig. 1b), with strengthened eddy activity occurring downstream (though it is important to note that the 500-hPa level lies within the planetary boundary layer over much of the plateau). The peak in $-\partial_y\overline{\theta}$ over subtropical Asia and the North Pacific is consistent with the strong westerly winds in thermal wind balance. Situated downstream of the Tibetan Plateau, eastern China (105°–120°E) is subject to relatively strong upstream baroclinicity. Transient eddy activity rapidly strengthens over eastern China (around 35°–45°N); the eddy geopotential variance is locally maximized in this region, consistent with enhanced frontal activity in the MB (Chen and Chang 1980; Ding et al. 2004; Ding and Chan 2005).

The present study investigates the interaction between extratropical eddies and low-level southerlies over eastern China during the summer monsoon season. In addition to being associated with NPSH variations, as discussed above, previous studies consistently indicate that the seasonal evolution and the interannual variability of the monsoon rainband are closely related to the position of the westerly jet over East Asia (Liang and Wang 1998; Zhou and Yu 2005; Sampe and Xie 2010; Chen et al. 2013; Li and Zhang 2014; Chiang et al. 2015). Here, we hypothesize that the seasonal-mean statistical relationship between the westerly jet position and the monsoon rainband is partly associated with the synoptic-scale eddy activity along the Asian westerly jet. In this study, we seek to elucidate the extratropical eddy effect on the EASM by considering the following questions:

1) What are the dynamic and thermodynamic characteristics of the synoptic eddy structure preceding the westward intensification of the NPSH and the associated strong monsoonal southerlies over eastern China?
2) How does upper-tropospheric wave propagation affect the low-level monsoon circulation?

To address these questions we perform lead–lag composite analysis preceding and following the anomalously strong monsoonal southerlies over eastern China. The rest of this paper is organized as follows. Section 2 describes the data and methodology used in our analysis. Then in section 3 we examine the surface pressure pattern associated with the strong southerly events over eastern China. In section 4, we examine the characteristics of upper-tropospheric wave propagation and its possible effect on the low-level monsoon circulation. In section 5, we seek to better understand the mechanisms of enhanced precipitation by evaluating the time evolution of dynamical lifting and moist stability over East Asia.

2. Data and methodology

a. Data

We use the European Centre for Medium-Range Weather Forecasts interim reanalysis (ERA-Interim) dataset (Dee et al. 2011). The reanalysis model comprises 60 vertical levels between the surface and about 65-km altitude with a horizontal resolution of about 80 km. The data products used in this study are 4× daily with a horizontal resolution of 1.5° × 1.5°. For our purposes, the data are averaged to daily means. We consider the 34-yr period spanning from 1979 to 2012.

Precipitation data are from the Global Precipitation Climatology Project (GPCP), which merges satellite-derived and in situ global precipitation data (Huffman et al. 2001). This GPCP dataset covers October 1996–December 2013 with 1.0° × 1.0° horizontal resolution and is archived at the National Center for Atmospheric Research (NCAR; ftp://ftp.cgd.ucar.edu/archive/PRECIP/). The time span of the GPCP data is ~17 yr shorter than that of ERA-Interim. The GPCP data are used primarily to demonstrate that many days (or episodes) of extreme precipitation over eastern China are associated with the development of strong southerlies (Figs. 2b,c).

b. Methodology

Lead–lag composite analyses are performed in order to investigate monsoonal southerly strengthening on short (~daily to weekly) time scales. For each grid point, seasonal cycles of the variables of interest are constructed from 30-day running averages of the 34-yr mean daily climatology for each calendar day. After deseasonalizing the data, interannual variability is removed by 2–120-day bandpass filtering. In this study, we focus on June and July because these two months are when the monsoonal southerlies over East Asia and the

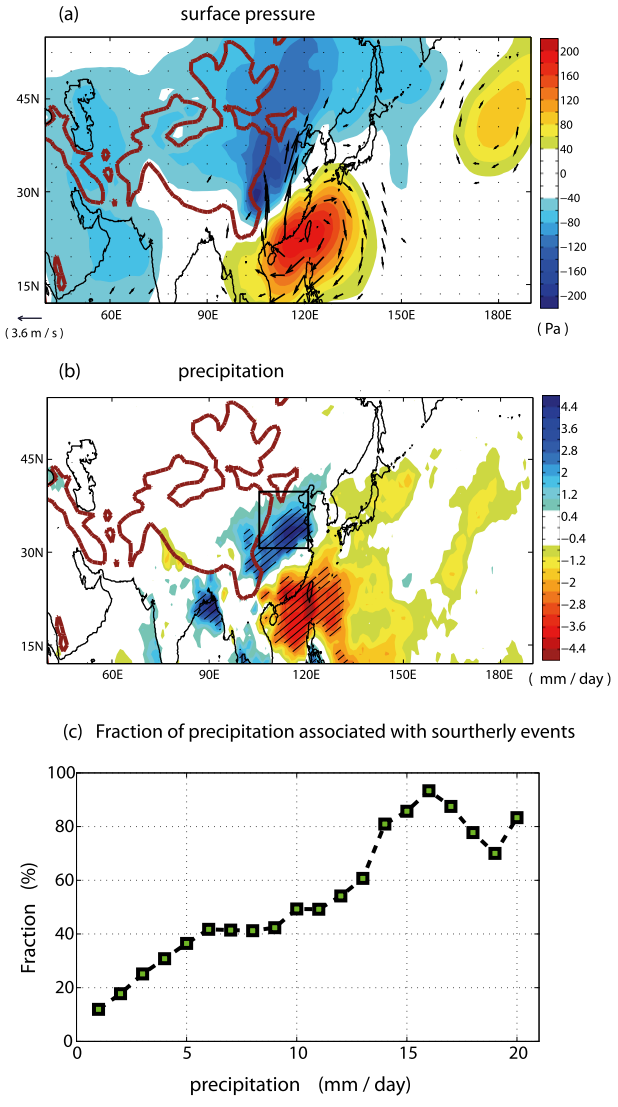

FIG. 2. June–July (a) composites of anomalous surface pressure (shadings; Pa) and anomalous 925-hPa winds (vectors; winds $>1.0\,\mathrm{m\,s^{-1}}$ are plotted) associated with strong southerly events during 1979–2012. (b) Composites of observed precipitation ($\mathrm{mm\,day^{-1}}$) associated with strong southerly events during 1997–2012. Statistically significant (*t* test: $p < 0.05$) values are hatched. (c) The fraction (%) of precipitation over eastern China (averaged over 30°–40°N and 105°–120°E) associated with strong southerly events during 1997–2012; the precipitation rate (abscissa) is binned by in $1\,\mathrm{mm\,day^{-1}}$ interval (e.g., the $10\,\mathrm{mm\,day^{-1}}$ tick corresponds to the precipitation rate between 9.5 and $10.5\,\mathrm{mm\,day^{-1}}$), and the fraction of days in that bin associated with southerly events is plotted. The black square box in (b) illustrates the averaging region for (c).

associated mei-yu rainband develop and ultimately peak (Zhou et al. 2009b; Molnar et al. 2010; Sampe and Xie 2010).

To define an anomalously strong southerly event, 925-hPa meridional wind anomalies (v) are zonally averaged over a longitude interval from 105° to 115°E. We further average over 20°–35°N, since southerly moisture flux over these latitudes accompanies precipitation over mainland China (Fig. 1c). Low-level southerly strengthening in this region is dynamically tied to the westward intensification of the NPSH and has been related to anomalously strong precipitation over eastern China (Wang et al. 2013). For our purposes, southerly events are defined as time periods during which area-averaged v exceeds 0.5 standard deviation over 3 or more consecutive days. Moreover, to assure temporal isolation of events, if the beginning of an event occurs within 6 days of the end of the preceding event, then the latter event is neglected. This procedure yields 72 distinct events for June and July over 1979–2012. Lag zero is defined as the day for which the area-averaged southerly wind amplitude peaks. Prior to generating the composites, a 3-day running average is applied to filter out noise associated with very high-frequency variability.

3. Development of southerlies and convection

a. Dipole pressure anomaly and precipitation

The composite surface pressure for strong southerly events over the mei-yu exhibits a land–sea dipole anomaly in surface pressure between eastern China and the South China Sea (Fig. 2a). This spatial distribution of anomalous surface pressure reinforces the climatological surface pressure pattern associated with the summertime land–sea thermal contrast—namely, low over the continent and high over the ocean. Anomalous high surface pressure over the South China Sea (red colors in Fig. 2a) can be interpreted in terms of the westward intensification of the NPSH, a well-known factor for strengthening the monsoonal southerlies (vectors in Fig. 2a) as shown in previous studies (Zhou et al. 2009a; Wu et al. 2010; Wang et al. 2013). However, relatively little attention has been given to the effect of extratropical lows (blue colors in Fig. 2a), which may also contribute to the southerly strengthening and potentially influence the westward intensification of the NPSH.

This dipole pressure anomaly is accompanied by anomalously strong precipitation over eastern China, especially over central China (Fig. 2b). This regional increase in precipitation is associated with below-normal rainfall over southern China, consistent with the observational analysis of Zou et al. (2010). Over eastern China, heavy precipitation events are largely associated with strong southerly events that transport moisture from the South China Sea into the continent. Figure 2c shows the percentage of precipitation days associated with strong southerly events over eastern

China, specifically over the region 30°–40°N, 105°–120°E where anomalous precipitation is maximized. The days experiencing strong southerly winds over eastern China are only about 26% of the total June–July days. Despite their relatively low frequency of occurrence, these strong southerly events explain about 45%–90% of heavy precipitation days ($>10\,\mathrm{mm\,day^{-1}}$). By contrast, less than 35% of weak precipitation days ($<5\,\mathrm{mm\,day^{-1}}$) occur during strong southerly events, suggesting that weak precipitation conditions are generally not associated with the large-scale monsoonal southerlies over eastern China. In the subsequent sections, we seek to diagnose the fundamental mechanisms that cause the southerly induced moisture convergence over eastern China by examining wave disturbances. For this, we perform lagged composite analyses to better understand the effect of extratropical waves on the development of monsoonal southerlies. We start by examining the propagation of extratropical surface lows over the Eurasian continent.

b. *Propagation of surface lows*

Figure 3 shows the composites of surface pressure in June and July from lag day −4 (i.e., pressure leading the peak southerlies by 4 days) to lag day 2. From this figure, it is clear that the development of southerlies over the mei-yu is associated with anomalous, southeastward-propagating extratropical surface low pressure centers. At day −4, the composite-mean surface low is located upstream over central Asia and Russia, between 40° and 60°N, and subsequently propagates southeastward along the northern and eastern margin of the Tibetan Plateau.

Concurrently, subtropical high perturbations over the western North Pacific and South China Sea are weak at day −4 but rapidly strengthen through day −2, leading to the development of monsoonal southerlies over eastern China. It is interesting to note that the anomalous southerlies first appear over central China at day −2. At day 0, the anomalous extratropical low and subtropical high are in closest proximity, with the latter peaking over the South China Sea. Approximately 2–3 days after the peak of monsoonal southerlies and the associated moisture convergence over eastern China, the surface low develops downstream (fourth row of Fig. 3). The development of an extratropical trough over East Asia has been hypothesized as a characteristic downstream Rossby wave response to diabatic heating in midlatitudes (Kaspi and Schneider 2013), although that is a time-mean response and here we are examining only one phase of a transient response. To summarize, the southeastward propagation of surface lows originating over central Asia, combined with the westward intensification of the NPSH, leads over time scales of days to about a week to the intensification of the mei-yu–baiu trough over East Asia.

4. Extratropical wave train

The propagation of anomalous surface low pressure can be interpreted as part of an extratropical wave train. In general, the extratropical wave train is clearly seen in the upper troposphere, where westerlies are much stronger and wave amplitude is generally larger. Previous studies have demonstrated that the EASM is affected by an upper-tropospheric wave train extending northwestward into central Asia and the Middle East (Enomoto et al. 2003; Kosaka et al. 2009). In what follows, we present evidence that rapid strengthening of monsoonal southerlies over eastern China is connected to the upper-tropospheric wave train.

a. *Wave train*

Figure 4 shows lagged composites of the upper-tropospheric (250 hPa) relative vorticity. During days −6 and −4, a zonally elongated wave train is evident from western Eurasia to East Asia (first row of Fig. 4). Here we see that, as part of an eastward-propagating transient wave train, an anomalously strong upper-tropospheric cyclone (rather than anticyclone) develops over eastern China (first and second row of Fig. 4) a few days before the peak southerly winds. This wave train also appears when regression analysis is used as an alternative to our compositing methodology (Fig. A1), verifying the robust relationship between low-level southerlies and upper-level wave disturbances on synoptic time scales. Although this wave train is a propagating, transient phenomenon, during days −6 and −4 it is reminiscent of the well-known regional summertime stationary wave called the Silk Road pattern (Enomoto et al. 2003; Kosaka et al. 2009). Specifically, cyclonic motion over eastern China and anticyclonic motion over central Asia are consistent with Fig. 2 of Kosaka et al. (2009). It is likely that these traveling waves interfere constructively with the quasi-stationary waves (i.e., Silk Road pattern) during the early stage of the strong southerly events.

The eastward propagation is better seen in a time–longitude Hovmöller plot of the meridional wind field at 250 hPa (Fig. 5), averaged over 35°–50°N.[1] The solid arrow overlaying the red shading, extending from 40° to 130°E over day −9 to day +7, highlights the phase propagation in the geopotential field. Following Yang

[1] The meridional average (from 35° to 50°N) encompasses higher latitudes than the region of the maximum upper-level cyclone over the eastern side of the Tibetan Plateau (around 35°–40°N). Since the wave train tends to propagate southeastward over Asia, the Hovmöller plot that includes higher latitudes better captures the eastward propagation of the wave train.

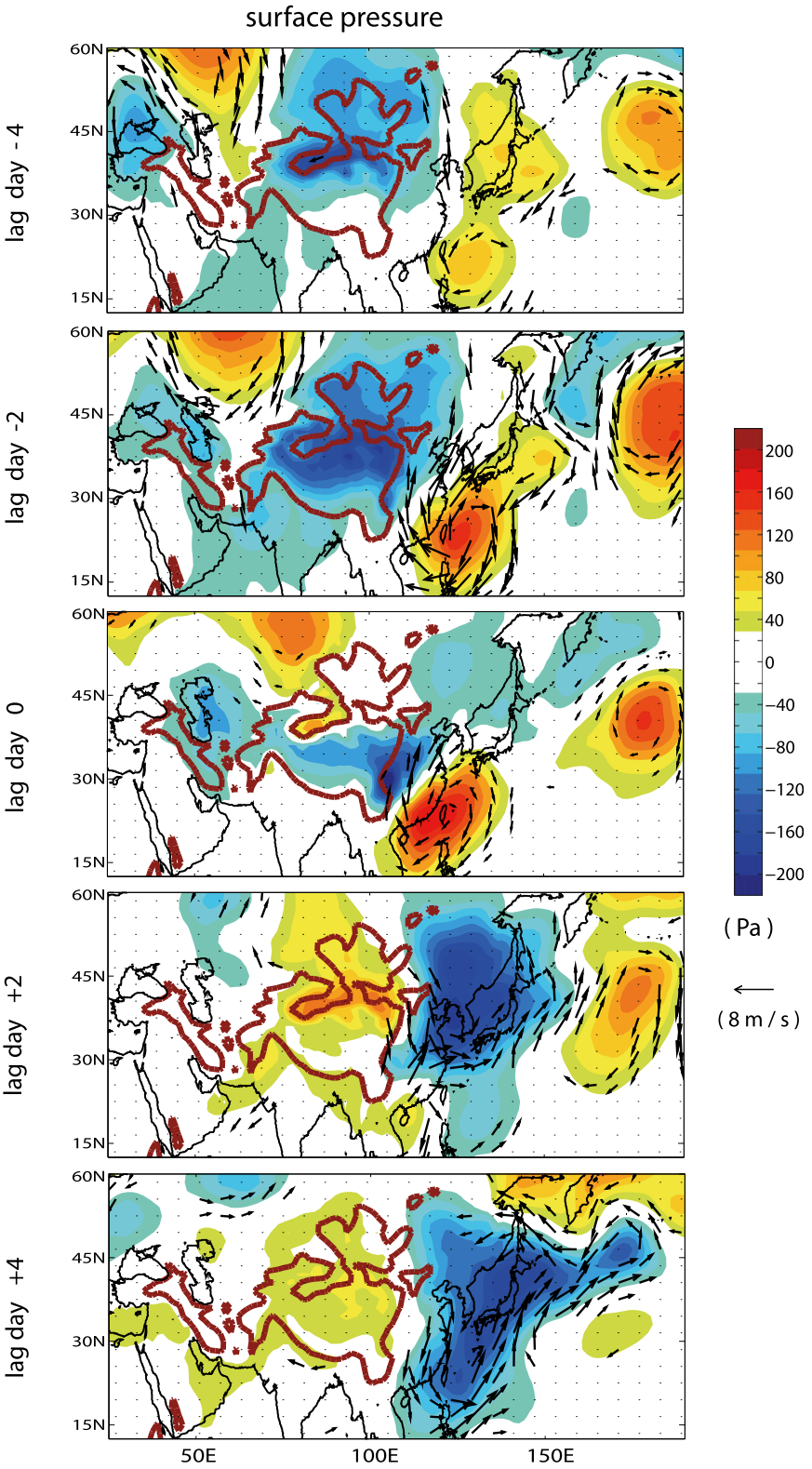

FIG. 3. Composites of anomalous surface pressure (shadings; Pa) for (top)–(bottom) lags −4, −2, 0, +2, and +4 days in June–July. Vectors are anomalous winds ($m\,s^{-1}$) at 925 hPa >1.0 $m\,s^{-1}$. The absolute values of anomalous surface pressure >100 Pa are mostly statistically significant (*t* test; $p < 0.05$).

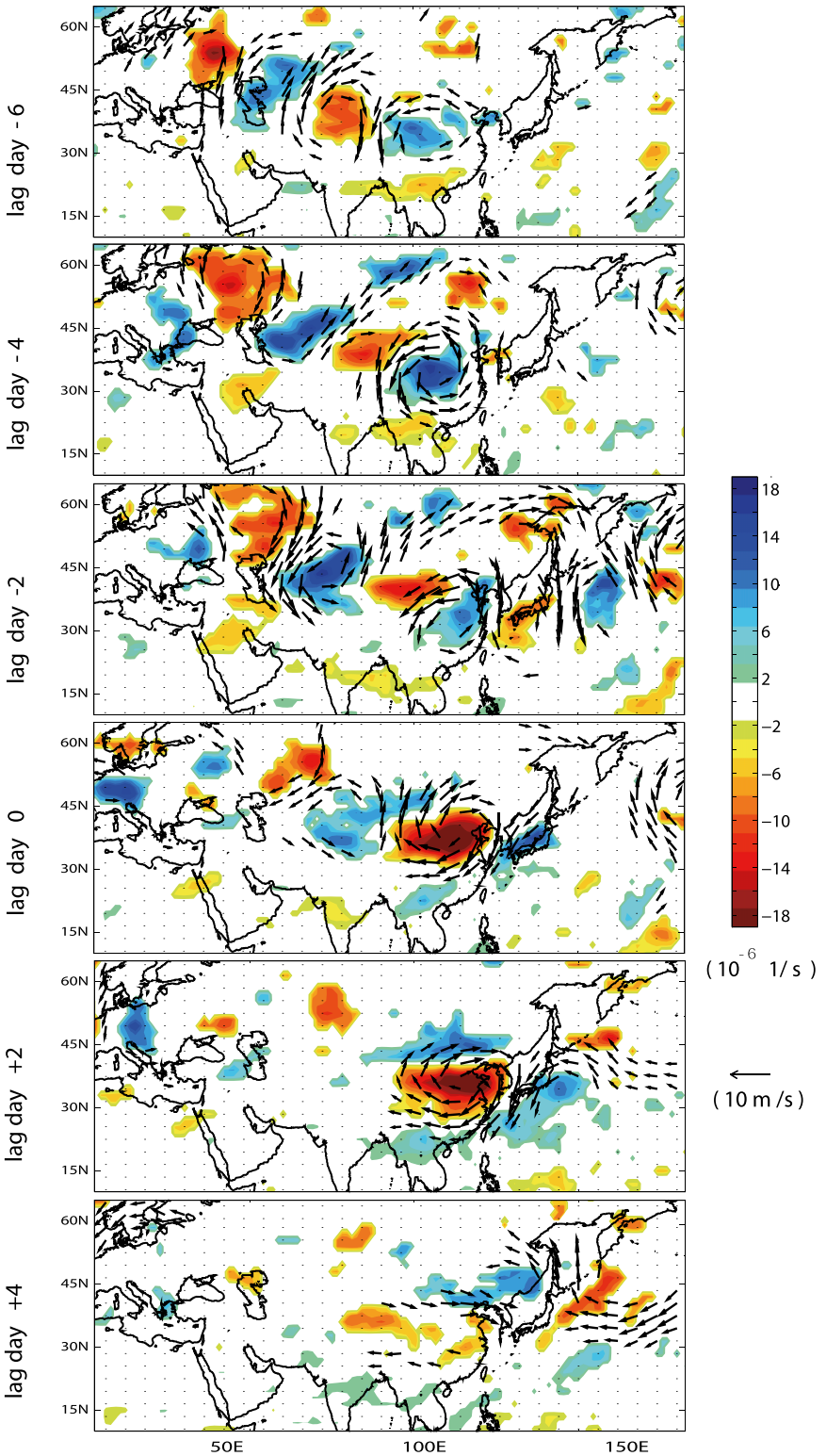

FIG. 4. Composites of anomalous relative vorticity (shadings; $10^{-6}\,s^{-1}$) with winds (vectors) at 250 hPa for (top)–(bottom) lags of −6 to +4 days in June–July. Only statistically significant values (t test; $p < 0.1$) are shaded and wind vectors >2.4 m s^{-1} are plotted.

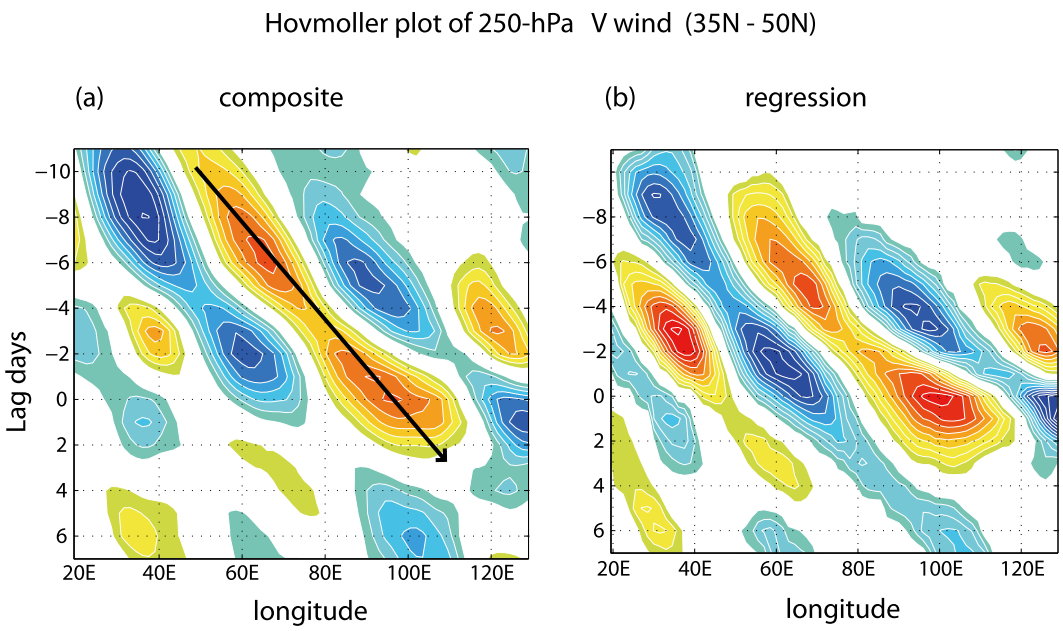

FIG. 5. Meridionally averaged (35°–50°N), longitude–time Hovmöller plot of anomalous meridional (V) winds ($\mathrm{m\,s^{-1}}$) at 250 hPa, based on the (a) composite and (b) regression analyses. The abscissa is longitude and the ordinate is the time lag associated with strong southerly wind events over eastern China. The solid line indicates the approximate zonal phase velocity of Rossby waves and is drawn subjectively. The contour intervals are 0.05 and $0.015\,\mathrm{m\,s^{-1}}$ in (a) and (b), respectively. The red (blue) color indicates anomalous northward (southward) flow.

and Hoskins (1996), the zonal phase speed of (barotropic) Rossby waves can be expressed as follows: $c = \overline{u} - \beta/(k^2 + l^2)$. Assuming a representative zonal wavenumber of synoptic-scale midlatitude eddies of $k \sim 7$ (Kiladis 1998), the zonal phase velocity c, over Asian midlatitudes, ranges from about 1.0 to $6.0\,\mathrm{m\,s^{-1}}$ at 250 hPa, depending on the mean westerly wind speed $\overline{u}$, which itself varies both meridionally and zonally. The phase velocity of the upper-level low inferred from Fig. 5 (solid line) is about $\sim 3.2\,\mathrm{m\,s^{-1}}$, which lies within the predicted range estimated from the simple dispersion relation.

The presence of an upper-level anticyclone (first row in Fig. 4 and second row in Fig. A1) over central Asia (northern part of the Tibetan Plateau) is reminiscent of the upper-level anticyclone over the Tibetan Plateau in several modeling studies, such as Wang et al. (2013). In Wang et al. (2008), a stationary wave train is generated by imposing heating over the Tibetan Plateau, so an enhanced upper-tropospheric anticyclone clearly appears over the Tibetan Plateau. On the other hand, Fig. 4 shows synoptic-scale traveling waves that are internally balanced with large-scale circulations. The upper-tropospheric cyclone situated along the eastern side of the Tibetan Plateau during days −4 and −2 is indicative of relatively high potential vorticity that is often associated with cold-air intrusions from higher latitudes (Aebischer and Schär 1998). This upper-tropospheric cyclone is rapidly replaced by an anticyclone from day −2 to day +2. This result is somewhat consistent with the upper-tropospheric vorticity transition following the penetration of extratropical wave trains into the South Pacific and South Atlantic convergence zones (Van der Wiel et al. 2015). As suggested by Van der Wiel et al. (2015), this upper-tropospheric anticyclone is dynamically tied to latent heating associated with deep convection (by creating upper-level mass divergence) from day 0 to day +2.

b. *Vertical structure*

The vertical structure of the extratropical wave train is depicted in the left column of Fig. 6 through the meridionally averaged (30°–40°N), longitude–height cross section of geopotential height anomalies. The height anomalies tilt westward with height, indicating poleward heat transport by the extratropical wave train. Consistent with Fig. 4, positive height anomalies appear over the western side of the Tibetan Plateau approximately 6 days before the monsoonal southerlies peak. Subsequently, anomalously low heights, especially in the upper troposphere, develop over the eastern side of the Tibetan Plateau and peak at day −4. This anomalously low height is consistent with the development of an upper-tropospheric cyclone at day −4 (Fig. 4). This anomalous geopotential height field is accompanied by changes in vertical motion (center column of Fig. 6).

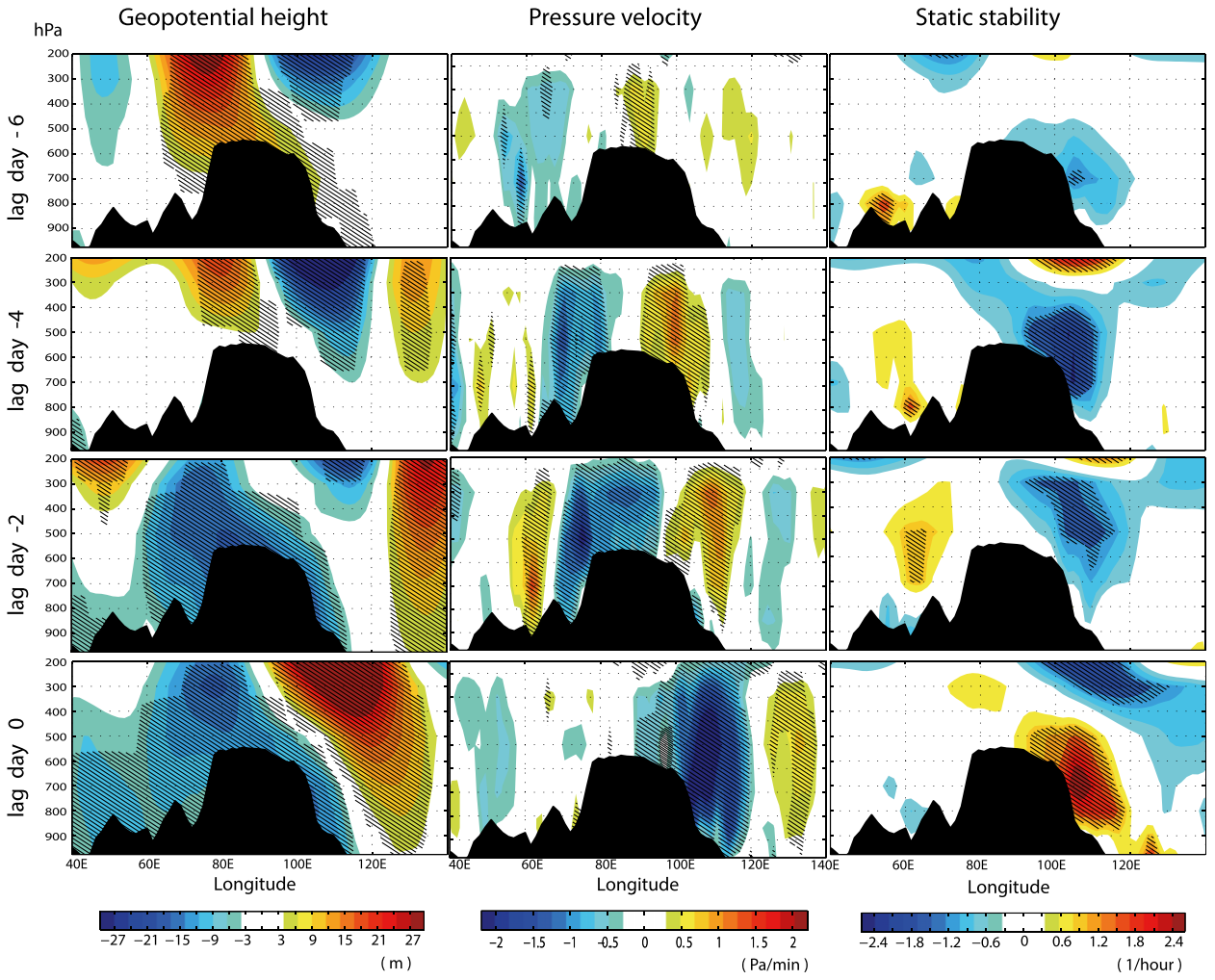

FIG. 6. Lagged composites of anomalous (left) geopotential height (m), (center) pressure velocity (Pa min^{-1}), and (right) static stability (h^{-1}) for (top)–(bottom) lag days of −6, −4, −2, and 0. The geopotential height and static stability are meridionally (latitudinally) averaged from 30° to 40°N. Statistically significant (*t* test: $p < 0.05$) values are hatched.

Specifically, anomalous ascent appears slightly west of anomalously high geopotential height, as expected for quasigeostrophic (QG) uplift in baroclinic waves in westerly vertical shear. This anomalous ascent is first seen west of the Tibetan Plateau and subsequently propagates eastward as part of the wave train. At days −2 and 0, when the monsoonal southerlies rapidly strengthen and peak, surface pressure decreases (Fig. 3), so temperatures near the Tibetan Plateau must be anomalously low, by hydrostatic balance; the anomalously low geopotential height (third and fourth rows of Fig. 6) verifies this balance.

The right column of Fig. 6 illustrates a measure of the static stability—namely, the Brunt–Väisälä frequency: $N = [(g/\theta)(d\theta/dz)]^{1/2}$. We now note that the wave train is associated with temporal variability in static stability. Over the eastern side of the Tibetan Plateau, where the upper-tropospheric geopotential height is relatively low, static stability substantially decreases in the mid- and lower troposphere (450–850 hPa) from day −6 through day −2. This reduced static stability is likely to be an initiating factor for the rapid strengthening of ascending motion over eastern China at day 0. This result suggests that the upper-level wave propagation can affect the mid- and lower-tropospheric circulations by changing static stability.

5. Moist QG lifting

a. QG omega equation

In this section, we attempt to better understand how the development of southerlies increases precipitation over eastern China. Specifically, we examine the dynamics

responsible for the uplift ($\omega < 0$) by using the full quasi-geostrophic omega equation:

$$\left(\sigma\nabla^2 + f_0^2\frac{\partial^2}{\partial p^2}\right)\omega = -2\nabla\cdot\mathbf{Q} - \frac{R}{p}\beta\frac{\partial T}{\partial x}, \qquad (1)$$

where ω is pressure velocity, β is the meridional gradient of the Coriolis parameter ($\beta = df/dy$), R is the gas constant, and $\sigma = \rho^{-1}\partial_p \ln\theta$ is a measure of static stability. We use an approximate form of $\nabla\cdot\mathbf{Q}$ in which the irrotational part of the horizontal wind is neglected:

$$\frac{p}{R}\nabla\cdot\mathbf{Q} \simeq \frac{\partial T}{\partial x}\frac{\partial \zeta}{\partial y} - \frac{\partial T}{\partial y}\frac{\partial \zeta}{\partial x} - \frac{\partial^2 T}{\partial x\partial y}\left(\frac{\partial^2\psi}{\partial x^2} - \frac{\partial^2\psi}{\partial y^2}\right) + \frac{\partial^2\psi}{\partial x\partial y}\left(\frac{\partial^2 T}{\partial x^2} - \frac{\partial^2 T}{\partial y^2}\right). \qquad (2)$$

Here, ζ is the vertical component of relative vorticity, ψ is the streamfunction of the horizontal wind, and T is temperature. This so-called **Q**-vector form (Hoskins et al. 1978) was used by Kiladis et al. (2006) in a study of African easterly waves and recently by Boos et al. (2015) in a study of Indian monsoon depressions. Following Boos et al. (2015), $-2\nabla\cdot\mathbf{Q}$ was computed for every 6-hourly period; these 6-hourly values were used to evaluate the composite means.

The composites of anomalous $-2\nabla\cdot\mathbf{Q}$ at 500 and 775 hPa, averaged from day 0 to day +1, are plotted in Figs. 7a and 7b, respectively. The dynamical forcing for vertical motion represented by $-2\nabla\cdot\mathbf{Q}$ incorporates the combined effects of horizontal temperature advection and advection of relative vorticity by the thermal wind. This term has a horizontal distribution that qualitatively matches the distribution of anomalous precipitation (cf. Figs. 7a,b with Fig. 2b), suggesting that QG lifting induces precipitation over eastern China. At 775 hPa, the **Q**-vector convergence ($-2\nabla\cdot\mathbf{Q} > 0$) peaks slightly south of the anomalously high precipitation. At 500 hPa, the **Q**-vector convergence shifts slightly to the north, and its magnitude is somewhat weaker than that at 775 hPa. The anomalous **Q**-vector convergence is thus tilted poleward with height, consistent with the fact that baroclinic waves are generally tilted poleward with height because of nongeostrophic effects (Yin and Battisti 2003). The second term on the right-hand side of Eq. (1) $[-[R/p)\beta(\partial T/\partial x)]$ represents the advection of planetary vorticity by the thermal wind; the fact that it is approximately 4 times smaller than the **Q**-vector convergence during strong southerly events indicates that the planetary vorticity gradient (i.e., the "beta" effect) is relatively unimportant compared to the effects of temperature and relative vorticity gradients for generating ascent in the wave train.

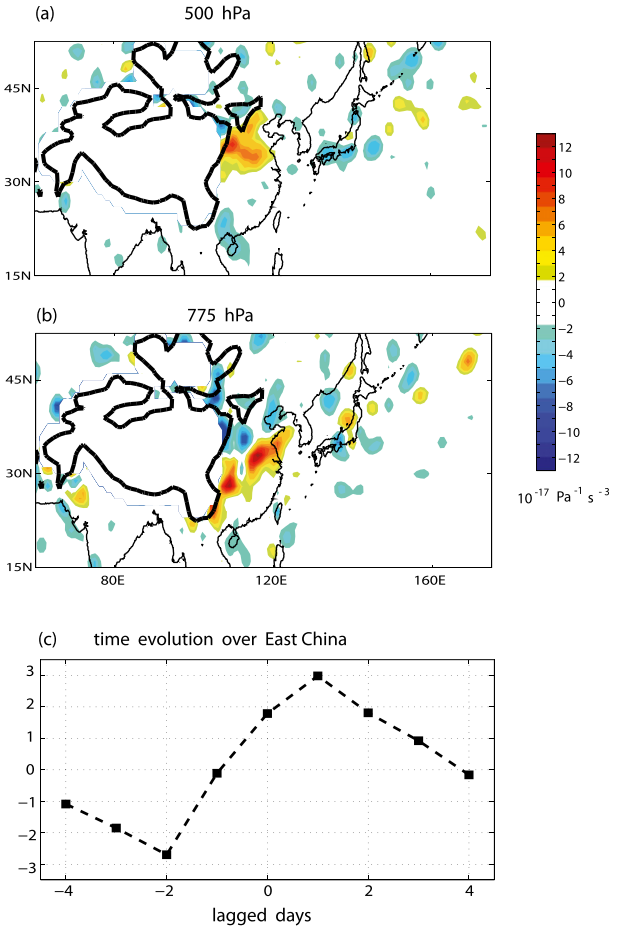

FIG. 7. Composite mean of dynamical forcing for ascent [$-2\nabla\cdot\mathbf{Q}$ of Eq. (1)] associated with strong southerly events at (a) 500 and (b) 775 hPa. Red (blue) colors indicate the forcing for ascent (subsidence). (c) Lagged composites of areal averaged $-2\nabla\cdot\mathbf{Q}$ over eastern China (30°–40°N, 105°–120°E). In (c), $-2\nabla\cdot\mathbf{Q}$ at 500 and 775 hPa are averaged (10^{-17} Pa^{-1} s^{-3}). In (a),(b), only statistically significant values (t test; $p < 0.1$) are color shaded.

Figure 7c shows lagged composites of $-2\nabla\cdot\mathbf{Q}$, area averaged over 30°–40°N and 105°–120°E, where the anomalous precipitation is largest (Fig. 2b). The development of surface lows and monsoonal southerlies from day −4 to day −1 is accompanied by the shift of $-2\nabla\cdot\mathbf{Q}$ from negative to positive. Several idealized modeling studies have produced a realistic NPSH and monsoonal southerlies by externally imposing condensational heating in the subtropics (e.g., Liu et al. 2001, 2004). However, strong episodes of monsoonal southerlies are clearly associated with baroclinic waves that interact with moist convection.

While QG forcing may initiate the uplift, latent heating associated with moist convection is expected to interact with dynamical lifting, thereby substantially altering ω (e.g., Boos et al. 2015). In other words, we have not inverted Eq. (1) to obtain a total vertical velocity field

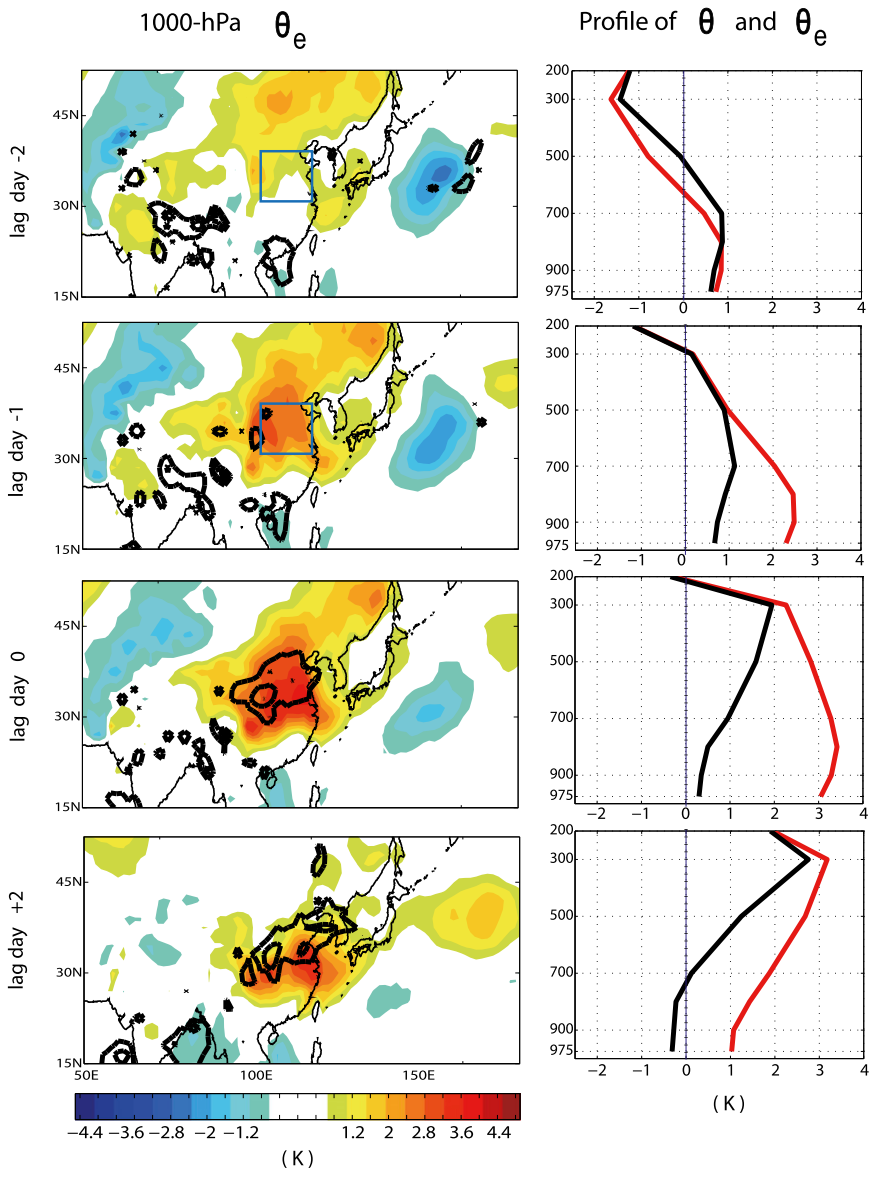

FIG. 8. Lagged composites of anomalous (left) 1000-hPa θ_e (K) and (right) areal averaged (30°–40°N, 105°–120°E) vertical profile of θ (black line) and θ_e (red line) for (top)–(bottom) days −2, −1, 0, and +2 . The blue square boxes in (left) illustrate the averaging region for (right).

because this would require assuming a temporally and spatially invariant dry static stability and neglecting the effects of moist convective heating on ω. In the next subsection, we examine the time evolution of near-surface θ_e, which may be relevant for the evolution of moist convection and its interaction with dynamical QG lifting.

b. *Moist stability*

The left column of Fig. 8 shows that anomalously strong precipitation over eastern China (contours in Fig. 8) at day 0 is largely coincident with the largest θ_e anomalies at 1000 hPa. Consistent with Fig. 6, the anomalous potential temperature θ (black line in the right column of Fig. 8) is negative in the mid- and upper troposphere at day −2 (day −4 is very similar to day −2 but is not shown), decreasing the static stability. At day −2, the vertical profiles of anomalous θ and equivalent potential temperature θ_e are very similar, indicating that moisture effects are small at this time. From day −2 to −1, near-surface θ_e rapidly increases and the vertical profile of θ_e substantially deviates from that of θ, most likely because of southerly induced moisture flux. The increase in low-level θ_e is

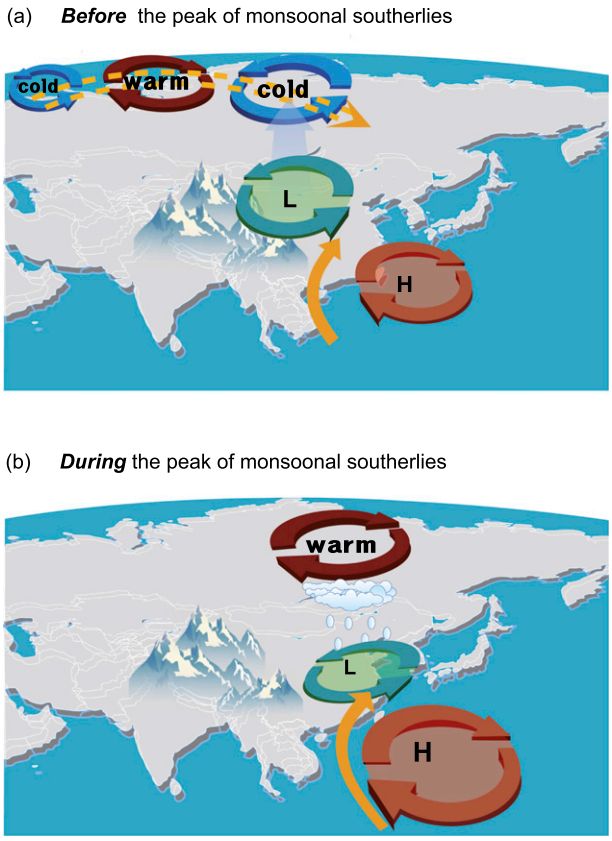

FIG. 9. Schematic illustrating the connection between the extratropical eddies and monsoonal southerlies on synoptic time scales (a) before and (b) during the peak of the monsoonal southerlies.

expected to be accompanied by an increase in convective available potential energy (CAPE), which would tend to foster enhanced moist convection and lead to a reduction in the "effective" static stability used in the QG omega Eq. (1). Prior studies (e.g., Sanders 1984) have attempted to account for the effects of moist convection in the QG omega equation by reducing the static stability to a fraction of its actual dry value. Although we do not make such a quantitative estimate here, we note that the reduction in dry static stability and the increase in CAPE that occur around day −2 and day −1 are both expected to aid in strengthening the QG uplift illustrated in Fig. 7. This suggests a picture of the extratropical wave train propagating to the southeast from western Eurasia and only producing intense precipitation when induced southerlies advect high-θ_e air and thus increase CAPE in the ascending part of the wave.

At day 0, θ_e in the lower troposphere maximizes, where areally averaged values of anomalous θ_e anomalies peak at 3.5 K. While heavy precipitation and associated latent heating rapidly increase upper-tropospheric temperatures and likely move the temperature profile toward a moist adiabat, θ_e in the lower troposphere may remain high enough to maintain positive CAPE and sustain the moist convection. By day +2, near-surface θ_e decreases and the θ profile warms even more at height, although heavy precipitation persists over eastern China and the Korea Peninsula along the mei-yu front. The areas of heaviest precipitation occur north of the highest 1000-hPa θ_e anomalies; one would not expect maxima in precipitation and θ_e to be aligned as they are in the more tropical South Asian monsoon (e.g., Boos and Emanuel 2009). Instead, precipitation and θ_e in this extratropical monsoon may be related via a baroclinic frontal zone. Several observational studies indicate that East Asian monsoon precipitation develops where the meridional gradient in low-level equivalent potential temperature $-d\theta_e/dy$ is maximized (Ninomiya 1984; Tomita 2011; Sampe and Xie 2010). This is probably because synoptic eddies can effectively mix moisture along isentropes (O'Gorman and Schneider 2006), leading to large-scale condensation along the mei-yu–baiu front.

6. Summary and discussion

Figure 9 provides a summary schematic illustrating how the westward intensification of the NPSH and the associated strengthening of monsoonal southerlies are dynamically tied to the extratropical wave train. The wave train propagates across Asia along the westerly jet, creating alternating cyclones and anticyclones with an upshear tilt in the vertical. QG vertical motion occurs throughout the wave train, but ascent is greatly amplified over eastern China where southerlies advect warm and moist air into the ascending part of the wave train, thereby creating heavy precipitation and upper-tropospheric anticyclones. Figure 9 thus provides a more detailed mechanistic view of the eddy activity and convective destabilization that have been suggested in prior work (e.g., Sampe and Xie 2010).

On seasonal time scales, the monsoon subtropical highs are known to be initiated by tropical or Asian continent heating. In contrast to the behavior on seasonal time scales, our study demonstrates that extratropical transient eddies can be an important factor influencing the monsoon circulation and diabatic heating field on synoptic time scales. The effect of a southeastward-propagating extratropical wave train on tropical convection is a classic example of tropical–extratropical interactions that are more typically documented in the winter and spring (Kiladis 1998). Our study suggests that this interaction still occurs in the early summer. On synoptic time scales, the upper-tropospheric wave train does not show clear evidence that it is associated with Tibetan Plateau heating (Wang et al. 2013) or the South Asian upper-tropospheric anticyclone (Wei et al. 2015). Here we document

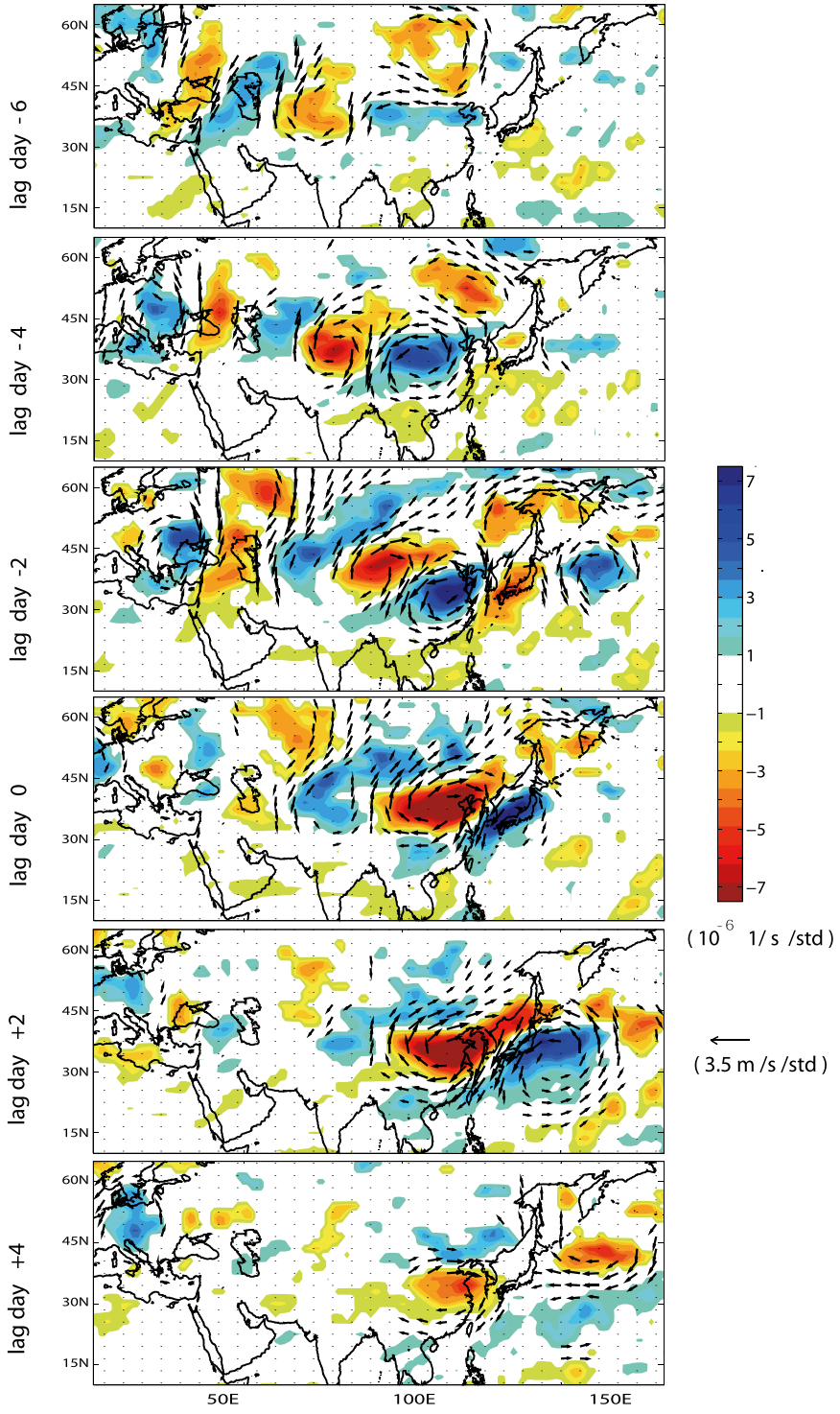

FIG. A1. Regression patterns of anomalous relative vorticity (shading; $10^{-6}\,s^{-1}$) with winds (vectors) at 250 hPa for (top)–(bottom) lags of −6 to +4 days in June–July. Only statistically significant values (t test; $p < 0.1$) are shaded and wind vectors $>0.8\,m\,s^{-1}$ are plotted.

anomalously warm (cold) conditions over the western (eastern) side of the Tibetan Plateau 6–7 days (2–4 days) prior to anomalous southerlies over eastern China. The upper-tropospheric cold-air advection over eastern China associated with the extratropical wave train decreases static stability in the mid- and lower troposphere. The timing of this reduced static stability is coincident with the timing of rapid increase in monsoonal southerlies and dynamical uplift by QG forcing.

So far, the westward intensification of the NPSH has been simply interpreted as a response to tropical or subtropical diabatic heating. While Wang et al. (2013) suggest that the NPSH variability is dynamically tied to the tropical diabatic heating, our results suggest that extratropical eddies could initiate its intensification on subseasonal time scales, especially over eastern China. Although diabatic heating is a major time-mean heat source affecting monsoonal southerlies, the westerly jet and the associated extratropical eddies might respond to the changes in diabatic heating field. As suggested by Miyasaka and Nakamura (2005), summertime subtropical circulations such as the NPSH should be understood in the context of the interactions between extratropical eddies and tropical diabatic heating. Our results suggest that monsoon prediction may be enhanced through better understanding of the patterns of extratropical wave trains (Kosaka et al. 2012; Song et al. 2013).

Acknowledgments. We thank Dr. Seok-Woo Son for helpful discussions and two anonymous reviewers for their constructive and insightful comments. HSP is supported by the Basic Research Project of the Korea Institute of Geoscience and Mineral Resources (KIGAM) funded by the Ministry of Knowledge Economy of Korea. KHS is supported by the Korean Meteorological Administration Research and Development Program under Grant CATER 2012-3071. WRB was supported by National Science Foundation Grant AGS-1253222.

APPENDIX

Regression Analysis

The upper-level wave train from the composite analysis, while statistically significant, is based on a limited number of strong southerly events (i.e., 72 events). To verify the relationship between the monsoonal low-level southerlies and upper-level wave train over Eurasia, we applied a simple linear regression analysis. Specifically, both the low-level (925 hPa) meridional wind over eastern China and the upper-level (250 hPa) relative vorticity as well as the wind field are filtered with a 2–30-day bandpass filter. This bandpass filtering removes the seasonal cycle and interannual variability. Then, the linear regression slope is calculated for each grid point. This procedure is almost identical to that of Kiladis and Weickmann (1992), except that Kiladis and Weickmann (1992) used a 2–20-day bandpass filter. The results we present (Fig. A1) are almost identical even if a 2–20-day bandpass filter is used.

Figure A1 shows the resulting wave train calculated from the simple linear regression analysis. The spatial pattern and the time evolution of this extratropical wave train are consistent with those from the composite analysis (Fig. 4). This result verifies that the monsoonal low-level southerlies over eastern China are dynamically tied to the upper-level wave train on synoptic time scales.

REFERENCES

Aebischer, U., and C. Schär, 1998: Low-level potential vorticity and cyclogenesis to the lee of the Alps. *J. Atmos. Sci.*, **55**, 186–207, doi:10.1175/1520-0469(1998)055<0186:LLPVAC>2.0.CO;2.

Boos, W. R., and K. A. Emanuel, 2009: Annual intensification of the Somali jet in a quasi-equilibrium framework: Observational composites. *Quart. J. Roy. Meteor. Soc.*, **135**, 319–335, doi:10.1002/qj.388.

——, J. V. Hurley, and V. S. Murthy, 2015: Adiabatic westward drift of Indian monsoon depressions. *Quart. J. Roy. Meteor. Soc.*, **141**, 1035–1048, doi:10.1002/qj.2454.

Chen, G.-S., R.-H. Huang, and L.-T. Zhou, 2013: Baroclinic instability of the Silk Road pattern induced by thermal damping. *J. Atmos. Sci.*, **70**, 2875–2893, doi:10.1175/JAS-D-12-0326.1.

Chen, T.-J. G., and C. P. Chang, 1980: The structure and vorticity budget of an early summer monsoon trough (meiyu) over southeastern China and Japan. *Mon. Wea. Rev.*, **108**, 942–953, doi:10.1175/1520-0493(1980)108<0942:TSAVBO>2.0.CO;2.

Chiang, J. C. H., and Coauthors, 2015: Role of seasonal transitions and westerly jets in East Asian paleoclimate. *Quat. Sci. Rev.*, **108**, 111–129, doi:10.1016/j.quascirev.2014.11.009.

Dee, D. P., and Coauthors, 2011: The ERA-Interim reanalysis: Configuration and performance of the data assimilation system. *Quart. J. Roy. Meteor. Soc.*, **137**, 553–597, doi:10.1002/qj.828.

Ding, Y., and J. C. L. Chan, 2005: The East Asian monsoon: An overview. *Meteor. Atmos. Phys.*, **89**, 117–142, doi:10.1007/s00703-005-0125-z.

——, C. Li, and Y. Liu, 2004: Overview of the South China Sea monsoon experiment. *Adv. Atmos. Sci.*, **21**, 343–360, doi:10.1007/BF02915563.

Enomoto, T., B. J. Hoskins, and Y. Matsuda, 2003: The formation mechanism of the Bonin high in August. *Quart. J. Roy. Meteor. Soc.*, **129**, 157–178, doi:10.1256/qj.01.211.

Hoskins, B. J., I. Draghici, and H. Davies, 1978: A new look at the ω-equation. *Quart. J. Roy. Meteor. Soc.*, **104**, 31–38, doi:10.1002/qj.49710443903.

Huffman, G., R. Adler, M. Morrissey, D. Bolvin, S. Curtis, R. Joyce, B. McGavock, and J. Susskind, 2001: Global precipitation at one-degree daily resolution from multisatellite observations. *J. Hydrometeor.*, **2**, 36–50, doi:10.1175/1525-7541(2001)002<0036:GPAODD>2.0.CO;2.

Kang, S., and J. Lu, 2012: Expansion of the Hadley cell under global warming: Winter versus summer. *J. Climate*, **25**, 8387–8393, doi:10.1175/JCLI-D-12-00323.1.

Kaspi, Y., and T. Schneider, 2013: The role of stationary eddies in shaping midlatitude storm tracks. *J. Atmos. Sci.*, **70**, 2596–2613, doi:10.1175/JAS-D-12-082.1.

Kiladis, G. N., 1998: Observations of Rossby waves linked to convection over the eastern tropical Pacific. *J. Atmos. Sci.*, **55**, 321–339, doi:10.1175/1520-0469(1998)055<0321:OORWLT>2.0.CO;2.

——, and K. M. Weickmann, 1992: Extratropical forcing of tropical Pacific convection during northern winter. *Mon. Wea. Rev.*, **120**, 1924–1938, doi:10.1175/1520-0493(1992)120<1924:EFOTPC>2.0.CO;2.

——, C. D. Thorncroft, and N. M. Hall, 2006: Three-dimensional structure and dynamics of African easterly waves. Part I: Observations. *J. Atmos. Sci.*, **63**, 2212–2230, doi:10.1175/JAS3741.1.

Knippertz, P., 2007: Tropical–extratropical interactions related to upper-level troughs at low latitudes. *Dyn. Atmos. Oceans*, **43**, 36–62, doi:10.1016/j.dynatmoce.2006.06.003.

Kodama, Y.-M., 1992: Large-scale common features of subtropical precipitation zones (the Baiu frontal zone, the SPCZ, and the SACZ). Part I: Characteristics of subtropical frontal zones. *J. Meteor. Soc. Japan*, **70**, 813–836.

Kosaka, Y., H. Nakamura, M. Watanabe, and M. Kimoto, 2009: Analysis on the dynamics of a wave-like teleconnection pattern along the summertime Asian jet based on a reanalysis dataset and climate model simulations. *J. Meteor. Soc. Japan*, **87**, 561–580, doi:10.2151/jmsj.87.561.

——, J. S. Chowdary, S.-P. Xie, Y.-M. Min, and J.-Y. Lee, 2012: Limitations of seasonal predictability for summer climate over East Asia and the northwestern Pacific. *J. Climate*, **25**, 7574–7589, doi:10.1175/JCLI-D-12-00009.1.

Li, L., and Y. Zhang, 2014: Effects of different configurations of the East Asian subtropical and polar front jets on precipitation during the mei-yu season. *J. Climate*, **27**, 6660–6672, doi:10.1175/JCLI-D-14-00021.1.

Li, S., J. Lu, G. Huang, and K. Hu, 2008: Tropical Indian Ocean basin warming and East Asian summer monsoon: A multiple AGCM study. *J. Climate*, **21**, 6080–6088, doi:10.1175/2008JCLI2433.1.

Liang, X.-Z., and W.-C. Wang, 1998: Associations between China monsoon rainfall and tropospheric jets. *Quart. J. Roy. Meteor. Soc.*, **124**, 2597–2623, doi:10.1002/qj.49712455204.

Liu, Y., G. X. Wu, H. Liu, and P. Liu, 2001: Condensation heating of the Asian summer monsoon and the subtropical anticyclone in the Eastern Hemisphere. *Climate Dyn.*, **17**, 327–338, doi:10.1007/s003820000117.

——, ——, and R. Ren, 2004: Relationship between the subtropical anticyclone and diabatic heating. *J. Climate*, **17**, 682–698, doi:10.1175/1520-0442(2004)017<0682:RBTSAA>2.0.CO;2.

Miyasaka, T., and H. Nakamura, 2005: Structure and formation mechanisms of the Northern Hemisphere summertime subtropical highs. *J. Climate*, **18**, 5046–5065, doi:10.1175/JCLI3599.1.

Molnar, P., W. R. Boos, and D. S. Battisti, 2010: Orographic controls on climate and paleoclimate of Asia: Thermal and mechanical roles of the Tibetan Plateau. *Annu. Rev. Earth Planet. Sci.*, **38**, 77–102, doi:10.1146/annurev-earth-040809-152456.

Ninomiya, K., 1984: Characteristics of baiu front as a predominant subtropical front in the summer Northern Hemisphere. *J. Meteor. Soc. Japan*, **62**, 880–894.

O'Gorman, P. A., and T. Schneider, 2006: Stochastic models for the kinematics of moisture transport and condensation in homogeneous turbulent flows. *J. Atmos. Sci.*, **63**, 2992–3005, doi:10.1175/JAS3794.1.

Rodwell, M. J., and B. J. Hoskins, 2001: Subtropical anticyclones and summer monsoons. *J. Climate*, **14**, 3192–3211, doi:10.1175/1520-0442(2001)014<3192:SAASM>2.0.CO;2.

Sampe, T., and S.-P. Xie, 2010: Large-scale dynamics of the meiyu-baiu rainband: Environmental forcing by westerly jet. *J. Climate*, **23**, 113–134, doi:10.1175/2009JCLI3128.1.

Sanders, F., 1984: Quasi-geostrophic diagnosis of the monsoon depression of 5–8 July 1979. *J. Atmos. Sci.*, **41**, 538–552, doi:10.1175/1520-0469(1984)041<0538:QGDOTM>2.0.CO;2.

Schiemann, R., D. Lüthi, and C. Schär, 2009: Seasonal and interannual variability of the westerly jet in the Tibetan Plateau region. *J. Climate*, **22**, 2940–2957, doi:10.1175/2008JCLI2625.1.

Seo, K.-H., J.-H. Son, S.-E. Lee, T. Tomita, and H.-S. Park, 2012: Mechanisms of an extraordinary East Asian summer monsoon event in July 2011. *Geophys. Res. Lett.*, **39**, L05704, doi:10.1029/2011GL050378.

Song, F. F., and T. J. Zhou, 2013: FGOALS-s2 simulation of upper-level jet streams over East Asia: Mean state bias and synoptic-scale transient eddy activity. *Adv. Atmos. Sci.*, **30**, 739–753, doi:10.1007/s00376-012-2212-7.

——, and ——, 2014a: The climatology and interannual variability of East Asian summer monsoon in CMIP5 coupled models: Does air–sea coupling improve the simulations? *J. Climate*, **27**, 8761–8777, doi:10.1175/JCLI-D-14-00396.1.

——, and ——, 2014b: Interannual variability of East Asian summer monsoon simulated by CMIP3 and CMIP5 AGCMs: Skill dependence on Indian Ocean–western Pacific anticyclone teleconnection. *J. Climate*, **27**, 1679–1697, doi:10.1175/JCLI-D-13-00248.1.

——, ——, and L. Wang, 2013: Two modes of the Silk Road pattern and their interannual variability simulated by LASG/IAP AGCM SAMIL2.0. *Adv. Atmos. Sci.*, **30**, 908–921, doi:10.1007/s00376-012-2145-1.

Ting, M. F., 1994: Maintenance of northern summer stationary waves in a GCM. *J. Atmos. Sci.*, **51**, 3286–3308, doi:10.1175/1520-0469(1994)051<3286:MONSSW>2.0.CO;2.

Tomita, T., 2011: Interannual variability of the baiu season near Japan evaluated from the equivalent potential temperature. *J. Meteor. Soc. Japan*, **89**, 517–537, doi:10.2151/jmsj.2011-507.

Van der Wiel, K., A. J. Matthews, D. P. Stevens, and M. M. Joshi, 2015: A dynamical framework for the origin of the diagonal South Pacific and South Atlantic convergence zones. *Quart. J. Roy. Meteor. Soc.*, **141**, 1997–2010, doi:10.1002/qj.2508.

Wang, B., 2006: *The Asian Monsoon*. Springer and Praxis Publishing, 788 pp.

——, R. Wu, and X. Fu, 2000: Pacific–East Asian teleconnection: How does ENSO affect East Asian climate? *J. Climate*, **13**, 1517–1536, doi:10.1175/1520-0442(2000)013<1517:PEATHD>2.0.CO;2.

——, Q. Bao, B. Hoskins, G. Wu, and Y. Liu, 2008: Tibetan Plateau warming and precipitation change in East Asia. *Geophys. Res. Lett.*, **35**, L14702, doi:10.1029/2008GL034330.

——, B. Xiang, and J.-Y. Lee, 2013: Subtropical high predictability establishes a promising way for monsoon and tropical storm predictions. *Proc. Natl. Acad. Sci. USA*, **110**, 2718–2722, doi:10.1073/pnas.1214626110.

Wei, W., R. Zhang, M. Wen, B. Kim, and J. Nam, 2015: Interannual variation of the South Asian high and its relation with Indian and East Asian summer monsoon rainfall. *J. Climate*, **28**, 2623–2634, doi:10.1175/JCLI-D-14-00454.1.

Wu, B., T. Li, and T. Zhou, 2010: Relative contributions of the Indian Ocean and local SST anomalies to the maintenance of the western North Pacific anomalous anticyclone during the El Niño decaying summer. *J. Climate*, **23**, 2974–2986, doi:10.1175/2010JCLI3300.1.

Wu, G., and Y. Liu, 2003: Summertime quadruplet heating pattern in the subtropics and the associated atmospheric circulation. *Geophys. Res. Lett.*, **30**, 1201, doi:10.1029/2002GL016209.

Yang, G.-Y., and B. J. Hoskins, 1996: Propagation of Rossby waves of nonzero frequency. *J. Atmos. Sci.*, **53**, 2365–2378, doi:10.1175/1520-0469(1996)053<2365:PORWON>2.0.CO;2.

Yang, J., Q. Liu, S.-P. Xie, Z. Liu, and L. Wu, 2007: Impact of the Indian Ocean SST basin mode on the Asian summer monsoon. *Geophys. Res. Lett.*, **34**, L02708, doi:10.1029/2006GL028571.

Yang, S., and P. J. Webster, 1990: The effect of summer tropical heating on the location and intensity of the extratropical westerly jet streams. *J. Geophys. Res.*, **95**, 18 705–18 721, doi:10.1029/JD095iD11p18705.

Yin, J. H., and D. S. Battisti, 2003: Why do baroclinic waves tilt poleward with height? *J. Atmos. Sci.*, **61**, 1454–1460, doi:10.1175/1520-0469(2004)061<1454:WDBWTP>2.0.CO;2.

Zhang, Y., X. Kuang, W. Guo, and T. Zhou, 2006: Seasonal evolution of the upper-tropospheric westerly jet core over East Asia. *Geophys. Res. Lett.*, **33**, L11708, doi:10.1029/2006GL026377.

Zhou, T., and R.-C. Yu, 2005: Atmospheric water vapor transport associated with typical anomalous summer rainfall patterns in China. *J. Geophys. Res.*, **110**, D08104, doi:10.1029/2004JD005413.

——, and Coauthors, 2009a: Why the western Pacific subtropical high has extended westward since the late 1970s. *J. Climate*, **22**, 2199–2215, doi:10.1175/2008JCLI2527.1.

——, D. Gong, J. Li, and B. Li, 2009b: Detecting and understanding the multi-decadal variability of the East Asian summer monsoon—Recent progress and state of affairs. *Meteor. Z.*, **18**, 455–467, doi:10.1127/0941-2948/2009/0396.

Zou, L., T. Zhou, L. Li, and J. Zhang, 2010: Eastern China summer rainfall variability of 1958–2000: Dynamical downscaling with a variable-resolution AGCM. *J. Climate*, **23**, 6394–6408, doi:10.1175/2010JCLI3689.1.